

# Tissue-Specific Transcription Footprinting Using RNA Pol DamID (RAPID) in *Caenorhabditis elegans*

Georgina Gómez-Saldivar,<sup>\*1</sup> Jaime Osuna-Luque,<sup>†,\*§,1</sup> Jennifer I. Semple,<sup>†</sup> Dominique A. Glauser,<sup>\*,2</sup> Sophie Jarriault,<sup>\*,2</sup> and Peter Meister<sup>†,2</sup>

<sup>\*</sup>Department of Biology, University of Fribourg, Fribourg 1700, Switzerland, <sup>†</sup>Cell Fate and Nuclear Organization, Institute of Cell Biology, University of Bern, 3012, Switzerland, <sup>‡</sup>IGBMC, DBSC Dept/INSERM U1258/CNRS UMR7104/Université de Strasbourg, 67400 France, and <sup>§</sup>Graduate School for Cellular and Biomedical Sciences, University of Bern, 3012, Switzerland

ORCID IDs: 0000-0003-3264-3222 (G.G.-S.); 0000-0001-5701-4129 (J.O.-L.); 0000-0001-7221-9560 (J.I.S.); 0000-0002-3228-7304 (D.A.G.); 0000-0003-2847-1675 (S.J.); 0000-0002-6230-4216 (P.M.)

**ABSTRACT** Differential gene expression across cell types underlies development and cell physiology in multicellular organisms. *Caenorhabditis elegans* is a powerful, extensively used model to address these biological questions. A remaining bottleneck relates to the difficulty to obtain comprehensive tissue-specific gene transcription data, since available methods are still challenging to execute and/or require large worm populations. Here, we introduce the RNA Polymerase DamID (RAPID) approach, in which the Dam methyltransferase is fused to a ubiquitous RNA polymerase subunit to create transcriptional footprints *via* methyl marks on the DNA of transcribed genes. To validate the method, we determined the polymerase footprints in whole animals, in sorted embryonic blastomeres and in different tissues from intact young adults by driving tissue-specific Dam fusion expression. We obtained meaningful transcriptional footprints in line with RNA-sequencing (RNA-seq) studies in whole animals or specific tissues. To challenge the sensitivity of RAPID and demonstrate its utility to determine novel tissue-specific transcriptional profiles, we determined the transcriptional footprints of the pair of XXX neuroendocrine cells, representing 0.2% of the somatic cell content of the animals. We identified 3901 candidate genes with putatively active transcription in XXX cells, including the few previously known markers for these cells. Using transcriptional reporters for a subset of new hits, we confirmed that the majority of them were expressed in XXX cells and identified novel XXX-specific markers. Taken together, our work establishes RAPID as a valid method for the determination of RNA polymerase footprints in specific tissues of *C. elegans* without the need for cell sorting or RNA tagging.

**KEYWORDS** single cell type gene expression analysis; *C. elegans* targeted DamID; RNA polymerase footprinting; ONT long read sequencing

**D**IFFERENTIAL gene expression across cell types encompasses both key determinants and markers of cell identity. Cataloging these differences can provide critical insights

and entry points in research aiming at elucidating the mechanisms controlling fundamental biological processes, such as organismal development and cell/tissue physiology. *Caenorhabditis elegans* is a widely used model animal, particularly well-suited for integrative studies bridging our understanding across the molecular, cellular, and organismal levels. With its transparent body, *C. elegans* was the first animal used to analyze tissue-specific transcription *in vivo* with GFP reporters (Chalfie *et al.* 1994), an approach still extensively used. In contrast to the versatility of the model for individual gene expression analysis, more holistic approaches such as tissue-specific transcriptomics still remain relatively challenging, in particular in postembryonic animals due to the tough cuticle and the difficulty to isolate intact tissue or cell types.

Two main general strategies have been developed to analyze specific tissues/cell types in *C. elegans*. A first general strategy involves the purification of tissue-specific messenger

Copyright © 2020 Gómez-Saldivar *et al.*  
doi: <https://doi.org/10.1534/genetics.120.303774>

Manuscript received August 17, 2020; accepted for publication October 9, 2020; published Early Online October 9, 2020.

Available freely online through the author-supported open access option.

This is an open-access article distributed under the terms of the Creative Commons Attribution 4.0 International License (<http://creativecommons.org/licenses/by/4.0/>), which permits unrestricted use, distribution, and reproduction in any medium, provided the original work is properly cited.

Supplemental material available at [figshare: https://doi.org/10.25386/genetics.13072355](https://doi.org/10.25386/genetics.13072355).

<sup>1</sup>These authors contributed equally to this work.

<sup>2</sup>Corresponding authors: University of Fribourg, Chemin du Musée 10, Fribourg, 1700, Switzerland. E-mail: dominique.glauser@unifr.ch; Institut de Génétique et de Biologie Moléculaire et Cellulaire, 1 rue Laurent Fries, 67400 Illkirch CU Strasbourg, France. E-mail: sophie@igbmc.fr; and University of Bern, Baltzerstrasse 4, Bern, 3012, Switzerland. E-mail: peter.meister@izb.unibe.ch

RNAs (mRNAs) from whole animals, which we will call “RNA tagging/pulling” hereafter. The most widely used RNA tagging/pulling method rely on the immunoprecipitation of a tagged poly-A binding protein-1 (FLAG::PAB-1) expressed in a specific cell type and cross-linked to RNA (Roy *et al.* 2002; Kunitomo *et al.* 2005; Pauli *et al.* 2006; Hrach *et al.* 2020). One of the latest versions of this method is referred to as polyA tagging and sequencing (PAT-seq; Blazie *et al.* 2015, 2017). The PAB-based method is technically demanding, in particular for the analysis of a small number of cells (Takayama *et al.* 2010) and has been shown to be associated with significant background noise (Von Stetina *et al.* 2007; Ma *et al.* 2016). Two more recent alternatives to PAB-based mRNA tagging are tissue-specific translating ribosome affinity purification (TRAP; Gracida and Calarco 2017; Rhoades *et al.* 2019) and *trans*-splicing-based RNA tagging (SRT; Ma *et al.* 2016). TRAP analysis focuses on ribosome-engaged mRNAs recovered after cross-linking and immunoprecipitation of a tagged ribosome subunit. TRAP allowed the identification of genes expressed in a specific neuron type representing only two cells per animal (Rhoades *et al.* 2019). SRT uses a modified SL1 splice leader expressed in target tissues, which is *trans*-spliced to the transcripts by the cellular machinery (Ma *et al.* 2016). While SRT bypasses the noise inherent in immunoprecipitation procedures, it has so far only been applied to large tissues and the approach is limited to SL1-associated transcripts (62% of the *C. elegans* genes; Yang *et al.* 2017).

The second general strategy relies on animal disruption and cell isolation, or dissociation, followed by the *in vitro* culturing or sorting of labeled cells (Von Stetina *et al.* 2007; Spencer *et al.* 2011), or nuclei (Haenni *et al.* 2012; Steiner *et al.* 2012) before transcriptomic analysis, and which we will call “dissociation-based” methods. The tough cuticle in larval stages and *a fortiori* in adults constitutes a significant obstacle, and initial studies focused on embryonic cells which were more easily dissociated. More recent protocols combining FACS and RNA-seq were successfully used to analyze major tissues (Kaletsky *et al.* 2018) as well as neuronal subsets in adults (Wang *et al.* 2015; down to six neurons per animal; Kaletsky *et al.* 2016). Combined with single-cell RNA-sequencing (scRNA-seq), large-scale dissociation-based studies can address transcript profiles in multiple cell types at the same time (Cao *et al.* 2017; Packer *et al.* 2019), including the analysis of individual neuron types (Hammarlund *et al.* 2018; Lorenzo *et al.* 2020). However, how efficiently specific cell types, especially rare cells, can be purified varies depending on their morphologies, how fragile they are, and the developmental stage considered, suggesting that dissociation-independent methods could be useful complementary approaches.

We investigated whether we could use DNA adenine methylation identification (DamID) to footprint actively transcribed genes in specific cell types in whole worms. This approach has been successfully used in *Drosophila* to determine transcribed genes in rare brain cell types (Southall *et al.* 2013). DamID relies on the low-level expression of a fusion between the *Escherichia coli* Dam methyltransferase and a

protein of interest, here a subunit of the RNA polymerase (Pol). Binding of the latter to DNA leads to the methylation of GATC sites in the vicinity of the binding site (Figure 1A). After DNA extraction, methylated GATCs are specifically cleaved by the restriction enzyme DpnI and amplified using adapter-mediated PCR before sequencing (Supplemental Material, Figure S1A). The adaptation of the method to *C. elegans* seemed promising since endogenous adenine methylation/demethylation is very rare in worms and not targeted to GATC motifs (Greer *et al.* 2015). Moreover, the GATC site frequency is expected to provide good spatial resolution. Indeed, *C. elegans* has 269,049 GATC sequences per haploid genome, corresponding to an average of one site for every 374 bp and a median of 210 bp (Gómez-Saldivar *et al.* 2016a). In *C. elegans*, DamID has been used to study the genomic footprint of the DAF-16 transcription factor (Schuster *et al.* 2010), and large-scale interactions between the genome and the nuclear periphery (Towbin *et al.* 2012; Sharma *et al.* 2014; Cabianca *et al.* 2019; Harr *et al.* 2020).

Here, we describe the RNA Polymerase DamID (RAPID) approach for transcriptional footprinting in specific tissues in *C. elegans* in both embryonic blastomeres and in young adults. Using a fusion between a small subunit present in all three RNA Pols, we show that the technique can be used on both fluorescently sorted blastomere cells and DNA isolated from entire young adults using cell-type-specific expression generated by *Cre/lox*. To test the versatility of the method, we determined the Pol footprints in three different tissues at each stage. In young adults, these tissues represent between 10 and 0.2% of the somatic cells of the animal. We show that meaningful transcriptional patterns can be recovered using this technique, in line with previously used RNA tagging/pulling and dissociation-based methods. We further explore how this technique can be used to discover tissue-specific markers and report the identification of eight new reporters expressed in adult XXX cells. Additionally, as a result of the phasing-out of older sequencers able to sequence amplicons of different sizes as produced by DamID-sequencing, we show that new long-read sequencing methods can be used to sequence DamID libraries, which makes it possible to carry out the experiments, from DNA extraction to amplicon sequencing, in less than a week, without any external sequencing facility.

## Materials and Methods

### Plasmids and transgenic strains

All plasmids and worm strains are listed in Tables S1 and S2. Tissue-specific DamID plasmids were generated using Gibson assembly. All DamID plasmids were integrated as single copies using MosSCI either on chromosome II or IV (see details in Table S1; Frøkjær-Jensen *et al.* 2008). Strains and plasmids are available upon request.

### Worm growth

Worms were grown on solid NGM, seeded with *OP50* bacteria for maintenance culture and genetic crosses. All worm

cultures were grown at 20°. For cell sorting, animals were grown on peptone plates seeded with HB101, synchronized twice by hypochlorite treatment. Young adults containing up to 10 embryos were recovered 66 hr after plating synchronized L1 larvae. For DamID experiments in young adults, worms were grown on NGM seeded with Dam-negative *E. coli* GM48 for at least two generations. Around 4000 synchronized L1s were seeded onto 100-mm plates (1000–1200 per plate) and collected 53 hr later. Worms were washed extensively with M9 (at least 10 times) and distributed in aliquots of 30  $\mu$ l, removing the excess liquid. Samples were snap-frozen and stored at –80°.

### **Sorting of embryonic blastomeres**

Synchronized gravid adult hermaphrodites containing 8–10 eggs were treated with hypochlorite. Eggs were then incubated for 3 hr in M9 at 25° until they reached the 1.5-fold stage. Eggs were transferred to 500  $\mu$ l egg buffer (25 mM HEPES pH 7.3, 118 mM NaCl, 48 mM KCl, 2 mM CaCl<sub>2</sub>, 2 mM MgCl<sub>2</sub>) and pelleted 1 min at 2000 rpm. The supernatant was then aspirated, leaving 100  $\mu$ l of buffer with the pellet. Then, 500 U of chitinase (C8241-25U; Sigma-Aldrich, St. Louis, MO) was added and the mixture was resuspended and further incubated for 1 hr at room temperature. Chitinase was neutralized with 800  $\mu$ l Leibovitz medium. Digested embryos were recovered by centrifugation at 3000 rpm for 5 min at 4°. Embryos were then dissociated into isolated blastomeres by pipetting up and down with a P1000 pipette, up to 150 times until dissociation was complete. The cell population was filtered with a Millex-SV syringe 5- $\mu$ m filter (SLSV025LS; Millipore, Bedford, MA). A total of 500 fluorescent cells (one technical replicate) were sorted using a BD FACSaria Fusion (8000 events/second; 85- $\mu$ m nozzle) in sterile PCR tubes containing 1  $\mu$ l of pick buffer (50 mM Tris-HCl, pH 8.3, 75 mM KCl, 3 mM MgCl<sub>2</sub>, 137 mM NaCl). Collected samples were then frozen in liquid nitrogen before further processing. After DamID processing and PCR (see below), two technical replicates were pooled for sequencing library preparation.

### **DamID amplification, library preparation, and sequencing**

For sorted cells, frozen samples were lysed by addition of 2  $\mu$ l of lysis buffer (10mM TrisAc, 10 mM MgAc, 50 mM KAc, 0.67% Tween 20, 0.67% Igepal + 1 mg/ml Proteinase K) and incubated for 2 hr at 60° before Proteinase K inactivation at 95° for 15 min. DamID amplicons were obtained as previously described (Gómez-Saldivar *et al.* 2016b), using 30 PCR cycles.

For young adults, DamID was performed on 500 ng gDNA extracted from the animals using DNeasy Blood and Tissue Kit (#69504; QIAGEN, Valencia, CA). Two replicates for each stage and cell type were processed. DamID amplicons were obtained as previously described (Gomez-Saldivar *et al.* 2016a), with 20 PCR cycles for worm-wide DamID, 22 PCR cycles for muscle DamID, 22–24 PCR cycles for intestine DamID, and 24–26 PCR cycles for DamID of XXX cells. New

Illumina patterned flow cell technology does not allow sequencing of amplicons larger than 600 bp. Both types of DamID PCR amplicons were therefore sequenced using nanopore sequencing. After AMPure XP (Beckman Coulter) purification with 1.8 bead volume, DamID PCR amplicons were directly used for nanopore library barcoding and preparation using NBD-104 and LSK-109 kits (Oxford Nanopore Technologies). Libraries were sequenced to obtain at least 1 million reads per library on MinION, using R9.4.1 flow cells. We compared the performance of both sequencing approaches by sequencing the same libraries with both old paired-end HiSeq2500 Illumina flow cells and nanopore sequencers. Coverage obtained by both approaches were similar (see snapshot of mapped reads in Figure S1E). However, nanopore sequencing allowed the direct sequencing of longer amplicons (Figure S1F), most likely because Illumina cluster amplification does not work well on molecules longer than 800 bp, even on old-generation (HiSeq2500) flow cells. We compared whole animal DamID sample libraries generated using previously described strains expressing either a free GFP-Dam fusion or a perinuclear lamin fusion (Sharma *et al.* 2014). Statistical comparison of both techniques at the single restriction fragment level gave a Pearson correlation coefficient between short paired-end (PE) and long reads between 0.84 and 0.86 (Figure S1G).

### **Bioinformatic analysis**

Nanopore sequences were base-called and demultiplexed using guppy 3.6 with the high-accuracy model, before mapping to the *ce11* genome using minimap2 (Li 2018). Reads were considered as DamID amplicons when both ends mapped  $\pm$ 8 bp from a genomic GATC motif. Filtered libraries were then used to call Pol footprinting values using the *damidseq\_pipeline* package (Marshall and Brand 2015), using bam files (parameters:–bamfiles–extend\_reads = 0). The *damidseq\_pipeline* normalizes for GATC accessibility using a free Dam (in our case Dam::GFP) profile. Per-gene values were extracted using *polii.gene.call* ([https://owenjm.github.io/damidseq\\_pipeline/](https://owenjm.github.io/damidseq_pipeline/)) with WS270 gene annotations. Correlations between libraries and methylation footprinting values were made using *ad hoc* R scripts available upon request. Normalized footprinting tracks were visualized using IGV. For the comparison with chromatin immunoprecipitation sequencing (ChIP-seq) tracks, fastq files were downloaded from the Gene Expression Omnibus (GEO), mapped to *ce11*, normalized for sequencing depth with a pseudocount of 8 and log<sub>2</sub>-normalized to the input. Final figure construction was made using IGV and Adobe Illustrator.

### **Array construction and microscopy**

Reporter plasmids were assembled using the three-fragment MultiSite Gateway system (Thermo Fisher Scientific). Promoters of candidate genes were PCR amplified from N2 genomic DNA. Primer sequences and promoter lengths are described in Table S3. Candidate promoters were cloned into pDONR-P4-P1R vector (Invitrogen, Carlsbad, CA) by

Gateway cloning, generating slot 1 entry vectors (Table S2). Final expression plasmids were generated by Gateway cloning between promoters (slot 1), mNeonGreen fluorescent ORF (slot 2; dg353; Hostettler *et al.* 2017), *unc-54* 3' UTR (slot 3; pMH473, gift from Marc Hammarlund), and pDEST-R4-R3. The control localization/expression plasmid [*sdf-9p::NLS::wrmScarlet*] was generated through a Gateway recombination reaction between dg801 (slot 1), dg651 (slot 2; Marques *et al.* 2019), pMH473 (slot 3), and pDEST-R4-R3. Finally, *promoter::mNeonGreen* and *sdf-9p::NLS::wrmScarlet* plasmids were co-injected into N2 young adult hermaphrodites at 20 ng/ $\mu$ l each, with 20 ng/ $\mu$ l of dg9 (*unc-122p::RFP*; red coelomocyte) as a co-injection marker (#8938; Addgene; Miyabayashi *et al.* 1999). Two stable lines of each candidate promoter were selected (Table S1). For imaging, young adult animals identified based on the red coelomocyte reporter expression were transferred to a 2% agarose pad containing 0.01% sodium azide. Worms were then imaged on a Zeiss Axiovert microscope with a  $\times 20$  objective driven by Visiview, using a Photometrics Coolsnap Myo CCD camera with GFP and RFP settings (60 planes spaced by 2  $\mu$ m), plus a middle plane section in DIC settings. Using Fiji, the acquired optical stacks were then partially z-projected to capture the worm section containing the XXX cells, identified using the *sdf-9p::NLS::wrmScarlet* signal. Final figure construction was made using Adobe Illustrator. For each promoter except *asp-9*, two independent extrachromosomal arrays were scored in at least five animals.

#### Identification of detected and unique tissue-specific genes and validation

Gene coverage of RAPID profiles are listed in Table S4 (blastomeres) and Table S5 (young adults) (Sheet 1–2). Detected genes in a tissue were defined as genes that are significantly expressed [false discovery rate (FDR) < 0.05] in one replicate of one tissue (Table S4, sheet 3 and Table S5, sheet 3). Genes consistently detected in a tissue were defined as genes that are significantly expressed (FDR < 0.05) in both replicates of one tissue (Table S4, sheet 4 and Table S5, sheet 4). Representative examples of consistently detected genes used in Figure 2C were selected from the CeNGEN project (*C. elegans* Neuronal Gene Expression Map & Network; <https://cengen.shinyapps.io/SCeNGEA/>; Hammarlund *et al.* 2018) and visualized using IGV (<https://igv.org/>).

Unique tissue-specific genes were defined as genes significantly and differentially expressed relative to the other two tissues (Table S4, sheet 5 and Table S5, sheet 5). Analysis of the uniqueness of the genes from each tissue was performed using the JavaScript library jvenn (<http://bioinfo.genotoul.fr/jvenn>).

To ensure an unbiased comparison between genes identified as expressed in muscle with RAPID and the set of genes identified with SRT (Ma *et al.* 2016), only SL1 *trans*-spliced genes were selected, based on the intersection with the 10,589 mRNAs annotated as SL1-*trans*-spliced by modENCODE (Allen *et al.* 2011), generating a subset of 3477 genes.

For the comparison between the genes identified in the intestine with RAPID and the set of genes identified with fluorescence-activated nuclear sorting (FANS; Haenni *et al.* 2012), downregulated genes were eliminated from the list and only genes found as expressed and upregulated (total 9169 genes) were analyzed. For the comparison between the genes identified with RAPID and the set of genes identified with FACS (Kaletsky *et al.* 2018) in muscle and intestine, we directly used the expressed genes list from Table S1, which contained 7690 and 9603 genes, respectively. Chi-squared statistical tests were performed using the GraphPad QuickCalcs (<https://www.graphpad.com/quickcalcs/contingency1/>; accessed August 2020).

#### Tissue-specific prediction analysis

Tissue expression prediction analyses were performed using the top 500 statistically significant genes that were uniquely enriched in muscle and intestine (Table S5, sheet 6), selecting a multigene search within the Tissue-specific Expression Predictions for *C. elegans* program, version 1.0 (<http://worm-tissue.princeton.edu/search/multi>). For the tissue expression prediction test using the RAPID muscle-SL1 group, the parameters published by Ma *et al.* (2016) were used.

#### Gene ontology analysis

Gene ontology (GO) analyses were performed on unique tissue-specific gene lists. GO terms and q-values were obtained using gProfiler (<https://biit.cs.ut.ee/gprofiler/gost>; version e100\_eg47\_p14\_7733820) with the g:SCS multiple testing correction method, applying a significance threshold of 0.05 (Table S5, sheet 7; Raudvere *et al.* 2019).

Functional enrichment analysis for genes detected with different methods was performed using WormCat (<http://www.wormcat.com/index>). Annotations classified into category 2 were visualized with heatmap diagrams.

#### Candidate selection for reporter analysis

Candidate genes were selected for follow-up promoter analyses with two goals in mind: demonstrating that they are indeed transcribed in XXX cells, and identifying markers with expression restricted to XXX cells. Since XXX cells represent only 0.2% of the *C. elegans* cellular content, we reasoned that XXX-specific markers should produce very little or no signal in the whole animal samples. Therefore, out of the 862 XXX-enriched genes, with a significant RAPID signal in XXX, but not in muscle or in intestine samples, we further removed genes detected in at least one worm-wide sample. We obtained a refined list of 275 XXX-marker gene candidates, which still included the known XXX cell markers *daf-9* and *eak-4* (Table S5, sheet 8). From this candidate list, we selected *dhs-17* as an uncharacterized gene with a plausible link to XXX cell function, plus 11 random candidates. To limit caveats related to operons, we excluded a candidate if another transcript was located <200 bp upstream. The XXX-specific RAPID signals (RNA Pol occupancy values) in the

12-gene subset (average = 1.35, SD = 0.59) were similar to those in the starting 275-gene set (average = 1.47, SD = 0.64;  $P = 0.16$  by Student's  $t$ -test).

### Data availability

Embryonic and adult DamID-sequencing data are available under the GEO accession number GSE157418. Supplemental material available at figshare: <https://doi.org/10.25386/genetics.13072355>.

## Results

### RNA Pol footprinting using RAPID

The RAPID approach relies on the expression of trace levels of the *E. coli* Dam fused to a subunit of the RNA Pols, and the analysis of its DNA occupancy to evaluate the transcriptional state of genes. We first tested whether we could use *AMA-1*, the largest catalytic subunit of RNA Pol II, as reported in targeted DamID, done in neuronal lineages in *Drosophila* (Southall *et al.* 2013). However, the Dam signal was too weak, possibly due to the fact that the expression level of this very large fusion protein under transcriptional control of the uninduced *hsp-16.2* promoter was too low (not shown), or that the localization of the Dam domain within the *C. elegans* Pol complex was not favorable to access its DNA substrate. We therefore replaced *AMA-1* with *RPB-6*, the *C. elegans* homolog of the RNA Pol subunit F present in all three RNA Pols (D. Katsanos, M. Ferrando-Marco, I. Razzaq, T. Southall, and M. Barkoulas; unpublished data). *RPB-6* together with *AMA-1* and *RPB-2*, forms a “clamp” that retains DNA near the active center of Pol II (Cramer *et al.* 2000), stabilizing the transcription on the DNA template. In contrast to *AMA-1* attempts, we obtained a strong DamID amplicon PCR signal in animals carrying a single-copy transgene of the *rpb-6::Dam* fusion. As these animals had not been subjected to heat shock, they therefore expressed only low levels of the Dam fusion, yet the methylation levels were sufficient to perform DamID. Amplicons were sequenced using an ONT MinION nanopore device (see *Materials and Methods* for details and experimental validation of the technique). After signal normalization with GFP::*Dam* data to control for overall chromatin accessibility, we could detect general patterns of methylation that were consistent with Pol-dependent methylation (Figure 1, D–F) and a good correlation at the gene level between replicates (Figure 1, B, D, and F). We compared the RAPID profiles with published recent RNA Pol II ChIP-seq data sets in young adult animals (Garrido-Lecca *et al.* 2016; Kalinava *et al.* 2017; Miki *et al.* 2017). Visually, the patterns appeared similar (see examples of profiles in Figure 1, D and F). Even if the nature of the data are not identical, we performed a comparative analysis between the data sets for all genes, downscaling the resolution of the ChIP-seq data to GATC fragment (Figure 1B). RAPID and RNA Pol ChIP-seq show

a significant correlation ( $R = 0.38$ – $0.46$ ). Overall, interreplicate correlations were higher between the RAPID replicates ( $R = 0.86$ ) and between the RNA Pol II ChIP-seq experiments ( $R = 0.63$ – $0.97$ ). The difference between the RAPID and RNA Pol II ChIP-seq profiles most likely results from the different approach to recover DNA and from the fact that RAPID in adults represent a picture of cumulative transcriptional activity, while the RNA Pol II ChIP-seq represents a Pol occupancy snapshot at the young adult stage.

To get a more quantitative understanding of the relation between RAPID and transcript abundance, we compared RAPID with RNA-seq data, using one of the published young adult RNA-seq data sets (Miki *et al.* 2017). We ranked all genes based on their RAPID signal and calculated the average RNA-seq signal across 30 equally sized bins. We observe a clear correlation between RAPID and RNA-seq: genes with high RAPID signal are highly expressed as determined by RNA-seq, while lowly expressed genes harbor low RAPID levels (Figure 1C).

To understand how the methylation signal spreads along the body of the genes, we constructed metagene plots over all 20,000 *C. elegans* genes for RAPID and RNA Pol II ChIP-seq experiments. ChIP-seq signals show a characteristic profile, as the Pol accumulates at the transcription start site (TSS) and the transcription end site (TES) (Figure 1E). RAPID signal increases steadily from the TSS to the TES, where it peaks before decreasing from the TES onward (Figure 1E). This 3' end accumulation is similar to the one observed in ChIP-seq. In contrast, the difference between ChIP-seq and RAPID profiles (absence of a 5' peak in RAPID) is very likely due to the localization of the *RPB-6::Dam* fusion inside the RNA Pol complex. Located on the opposite side of the *AMA-1/RPB-2* complex relative to the DNA strands, the presence of the preinitiation complex at the promoter greatly restricts access to DNA [for review, see Cramer (2004); Schier and Taatjes 2020]. Once the Pol switches to elongation, leaving the preinitiation complex on the promoter, Dam is likely to gain access to the DNA and efficiently methylates the transcribed region, as observed in the RAPID profiles.

We also examined the profile in genes transcribed by Pol I and Pol III. As expected from the differential inclusion of *AMA-1* and *RPB-6* subunits in the different Pols, RAPID with *RPB-6* also labeled genes transcribed by RNA Pol I and III. RAPID showed high enrichments on the ribosomal RNA genes at the end of chromosome I (Figure S2A), as well as a majority of previously characterized small nucleolar RNAs (snoRNAs) transcribed by RNA Pol III (46 out of 57; Ikegami and Lieb 2013). snoRNA are sometimes located in introns of Pol II-transcribed genes, making it difficult to differentiate whether the RAPID signal originates from the snoRNA transcription or from the overlapping gene. Nevertheless, 24 out of 44 RAPID-positive snoRNA genes could be unambiguously assigned to Pol III transcription as there was no overlap (Figure S2B). In contrast, the corresponding signal was markedly weaker in the young adult RNA Pol II ChIP-seq data sets and very high for the RNA Pol III subunit *RPC-1* (performed in embryos, Figure S2B; Ikegami and Lieb 2013).

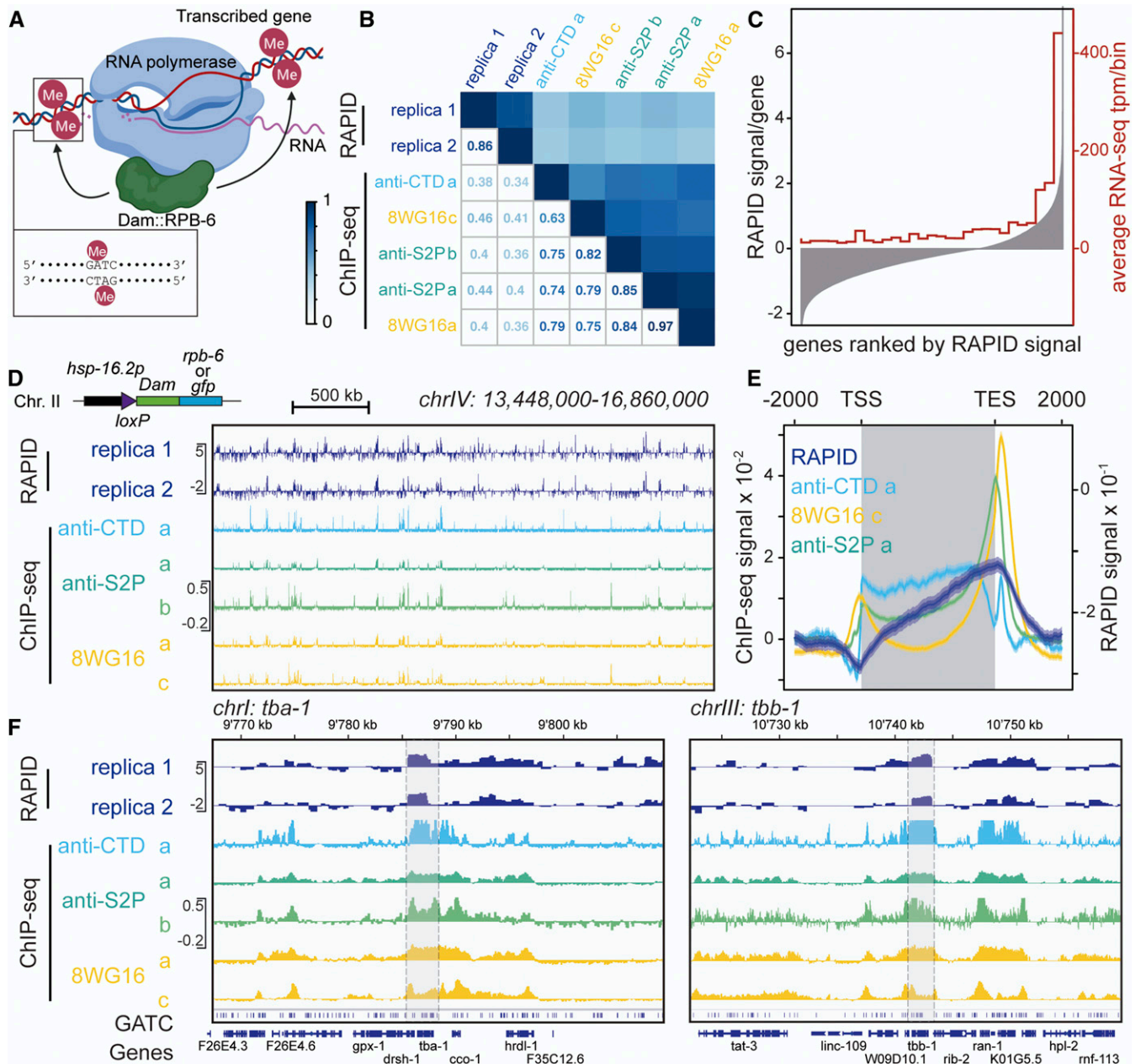


**Figure 1** RAPID: RNA Pol II DamID scheme. (A) *Dam::rpb-6* bound to all three RNA polymerase types modifies proximal GATC motifs. DamID analysis provides RNA polymerase footprints *in vivo*. (B) Gene-level correlations in young adult whole animals of RAPID and RNA polymerase ChIP-seq using different antibodies [a: Garrido-Lecca *et al.* (2016); b: Kalinava *et al.* (2017); c: Miki *et al.* (2017)]. (C) Comparison of RAPID signal with mRNA expression profiling. All genes are represented on the x-axis, ranked from left to right, based on RAPID signal in the entire animal (shown on left y-axis). Average transcripts per million (tpm; calculated with salmon) using data set from study c above (ribosomal RNA depleted) were calculated, using the genes falling into each bin of 690 genes on the x-axis (values on right y-axis). (D and F). Profiles at large scale (D) and gene scale (housekeeping genes, F) of RAPID and the different RNA polymerase II ChIP-seq studies cited in B. (E) Metagenome plot of the RNA polymerase II ChIP-seq and RAPID signals on WS270 genes. TES, transcription end site; TSS, transcription start site.

Taken together, these data show that the RAPID method is suitable to reveal RNA Pol footprints, serving as indirect indications of transcriptional activity by the three different RNA Pols.

#### RAPID in FACS-sorted embryonic cells

Since RAPID could label transcribed genes in whole animals, our next goal was to adapt the method for tissue-specific

analysis. We first explored whether RAPID could be used to footprint transcription in specific cell types of the embryo purified using fluorescence sorting. Using strains constitutively expressing *Dam* fusions, we sorted 1000 cells for 3 different tissues of various abundance: body wall muscle, intestine, and the rectal Y cell (80, 20, and 1 cell per embryo, respectively; Figure S3A and Table S4). RAPID could produce

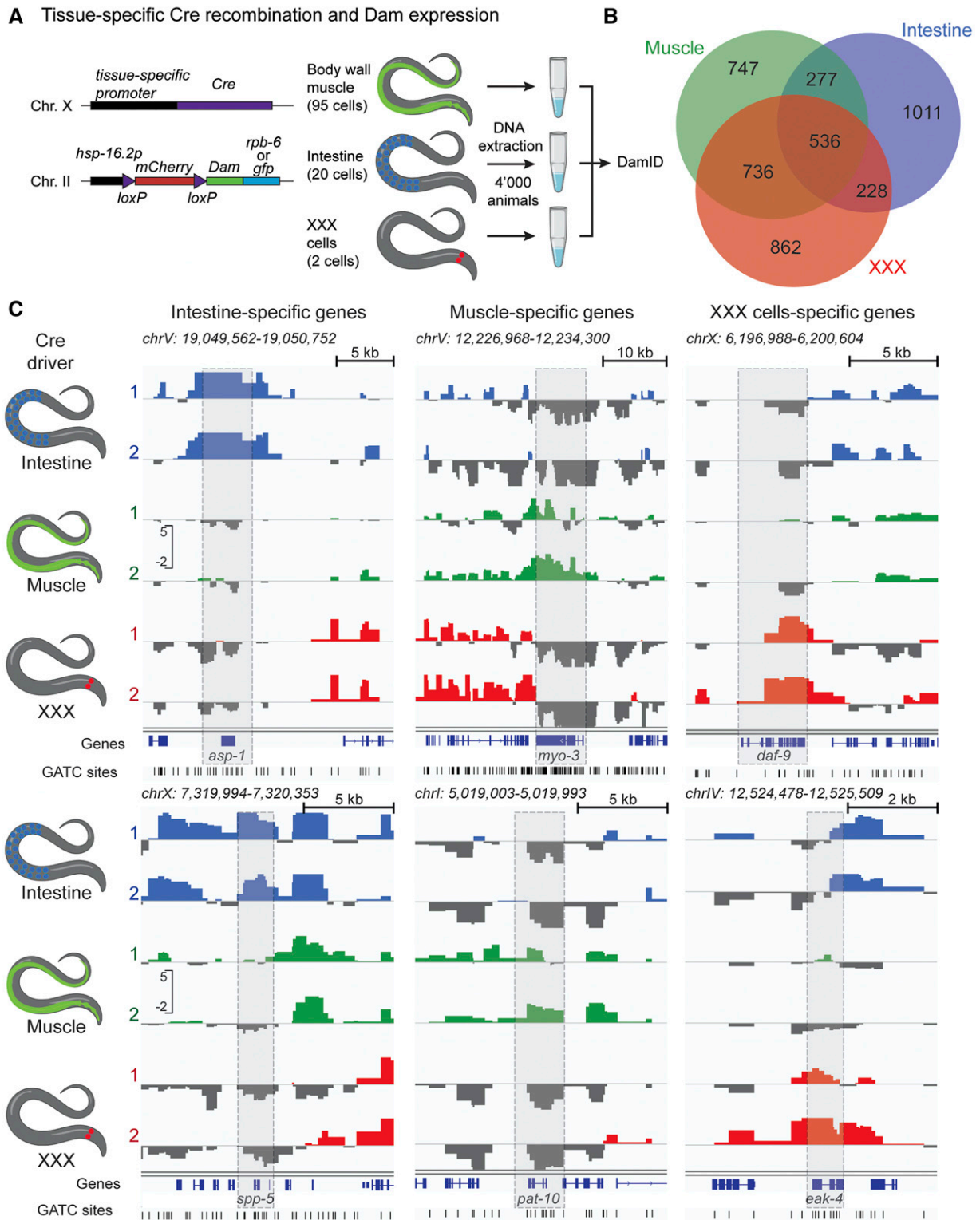


**Figure 2** Tissue-specific expression profiles using RAPID by Cre/lox recombination in young adult animals. (A) Experimental system for tissue-specific expression of Dam fusions and RAPID analysis. (B) Venn diagram of overlap between expressed genes identified using RAPID in three different tissues. (C) RAPID profiles for previously characterized genes expressed in a tissue-specific manner in intestine, muscle, and the XXX neuroendocrine pair.

footprints for all samples (Figure S3C), and the reproducibility of the RAPID signal at the gene level between replicas was good for the intestinal sample ( $r = 0.78$ ) but lower for muscle

and Y cell samples ( $r = 0.46$  and  $0.24$ , respectively; Figure S4A). When using an FDR  $< 0.05$ , we detected a total of 4986, 3165, and 4819 genes with a high RAPID signal in

the muscle, intestinal, and Y data sets, respectively; and 1566, 1570, and 840 consistently detected genes (FDR < 0.05 in both replicates) in these tissues (Table S4). In these experimental conditions, RAPID appears suitable to identify transcription footprints of cell-type-specific genes, such as the intestinal genes *cpr-6* (cathepsin B; Pauli *et al.* 2006) and *elo-2* (fatty acid elongase ELOVL; Han *et al.* 2017), or the Glutathione S-Transferase gene *gst-4* expressed in muscle, as well as the muscle-specific WDR1 homolog *unc-78* (Figure S3C; Mohri and Ono 2003; Hasegawa *et al.* 2007). Comparison of the footprints obtained for all three tissues allowed us to define 395 Y-specific genes (Figure S3B), and among them, shallow Y-specific RAPID signal was visible for *ceh-6* and *sox-2*, two transcription factors previously shown to be involved in Y-to-PDA transdifferentiation initiation (Figure S3C; Kagias *et al.* 2012). In contrast, we observed some unexpected RAPID footprints for genes that we expected to be expressed in a tissue-specific manner. For example, the myosin *myo-3* was observed in all three tissues (Figure S3D). Conversely, some genes which are known to be expressed in tissue-specific manner did not show high RAPID values, e.g., the intestine-specific *asp-1* and *spp-5* genes or the muscle-specific *pat-10* gene (Figure S3D). These differences might have a biological significance: most transcription patterns have been defined in older animals, yet those genes might be expressed more broadly, or not at all, in embryonic blastomeres. Alternatively, the lack of a robustly established transcription pattern might hinder faithful footprinting. Indeed, RAPID requires the enzymatic action of the methyltransferase to build up the signal, while footprints are removed at each replication round in rapidly dividing blastomeres. Together with the stochasticity of single methylation events, this might decrease the precision of the profiles. In agreement with this, intestinal cells, most of which are born and remain postmitotic early, display high reproducibility in the RAPID signal, while late-born muscle and the Y cell are less reproducible (Figure S3, C and D). In conclusion, RAPID allows transcriptional footprinting of sorted cells, provided cells have been born long enough for the Dam fusions to methylate reproducibly their target genes. These results thus suggest that RAPID may be more suited for the study of later developmental stages.

### **Tissue-specific RAPID in young adult animals**

We next asked whether we could use the RAPID approach for the analysis of tissue-specific transcription profiles in adult worms. To circumvent the technical difficulties associated with mature animal dissociation and cell sorting, we sought to implement a transgenic approach for the cell-specific targeting of the RPB-6::Dam fusion. Several strategies have been developed to target Dam fusion expression to specific tissues, using either bicistronic constructs attenuating Dam translation (Southall *et al.* 2013), tamoxifen-induced nuclear translocation (Pindyurin *et al.* 2016; Redolfi *et al.* 2019), or tissue-specific recombination cassettes (Muñoz-Jiménez *et al.* 2017). We used the latter strategy using an insertion of a floxed mCherry

ORF located between the *hsp-16.2* promoter and the Dam fusion (Figure 2A). Tissue-specific expression of the Cre recombinase leads to low-level expression of the Dam fusion (Ruijtenberg and van den Heuvel 2015). We used three different Cre drivers expressed in muscle, intestine, and a pair of head neuroendocrine cells called XXX, using *myo-3*, *elt-2*, and *sdf-9* promoters, respectively. We conducted cell-specific RAPID with only 4000 young adult hermaphrodites as starting material for DNA extraction. DamID signal across genes was highly correlated between replicates, and less correlated between different Cre drivers, suggesting tissue-specific DamID footprinting (Figure S4B).

Among the genes with high RAPID signal, we defined sets of detected genes in each tissue (with an FDR < 0.05 in at least one replicate), representing 4379, 4583, and 3901 genes with high RAPID footprint in intestine, muscle, and XXX cells, respectively. Among these, we also defined sets of consistently detected genes (with an FDR < 0.05 in both replicates), encompassing 2052, 2296, and 2362 genes in intestine, muscle, and XXX cells, respectively. Out of these, 1011, 747, and 862 were detected in only one tissue and defined as tissue-specific (Figure 2B, Table S5, sheet 5). A total of 536 genes harbored high RAPID footprints in all three sampled tissues (Figure 2B, Table S5, sheet 9), and a GO term analysis highlighted many very general terms consistent with the function of housekeeping genes (Table S5).

We validated these results focusing first on individual genes with well-characterized, tissue-specific expression (Figure 2C). The intestine-specific progastricsin aspartyl protease homolog gene *asp-1* and the saposin-like channel defense gene *spp-5* were exclusively footprinted in intestinal samples (Tcherepanova *et al.* 2000; Roeder *et al.* 2010). *myo-3*, the muscle myosin gene and *pat-10*, a troponin gene, both exclusively expressed in muscle tissues, harbored high RAPID footprints in muscle samples (Miller *et al.* 1986; Kagawa *et al.* 1997). Finally, the XXX-specific genes *daf-9* (encoding a P450 cytochrome homolog) and *eak-4* (encoding a membrane protein) were marked with RAPID exclusively in XXX cells (Gerisch *et al.* 2001; Hu *et al.* 2006).

### **Comparison of tissue-specific RAPID with available data sets in muscle and intestine**

To expand the validation of our RAPID footprint gene lists beyond selected tissue markers, we next engaged three more comprehensive approaches. These approaches focused on muscle and intestine, since no large-scale gene expression data are available in XXX cells.

First, we focused on a narrower set of genes with high RAPID footprints present exclusively in one of the tissues. These gene lists with the top 500 unique genes of each tissue, were analyzed with a computational method that predicts tissue-specific enrichment, using a multigene query (<http://worm-tissue.princeton.edu/>; Chikina *et al.* 2009). The tissue prediction tool showed that muscle-only and intestine-only RAPID footprinted genes gave a high prediction score for muscle and intestine, respectively (Figure 3, A and B). In



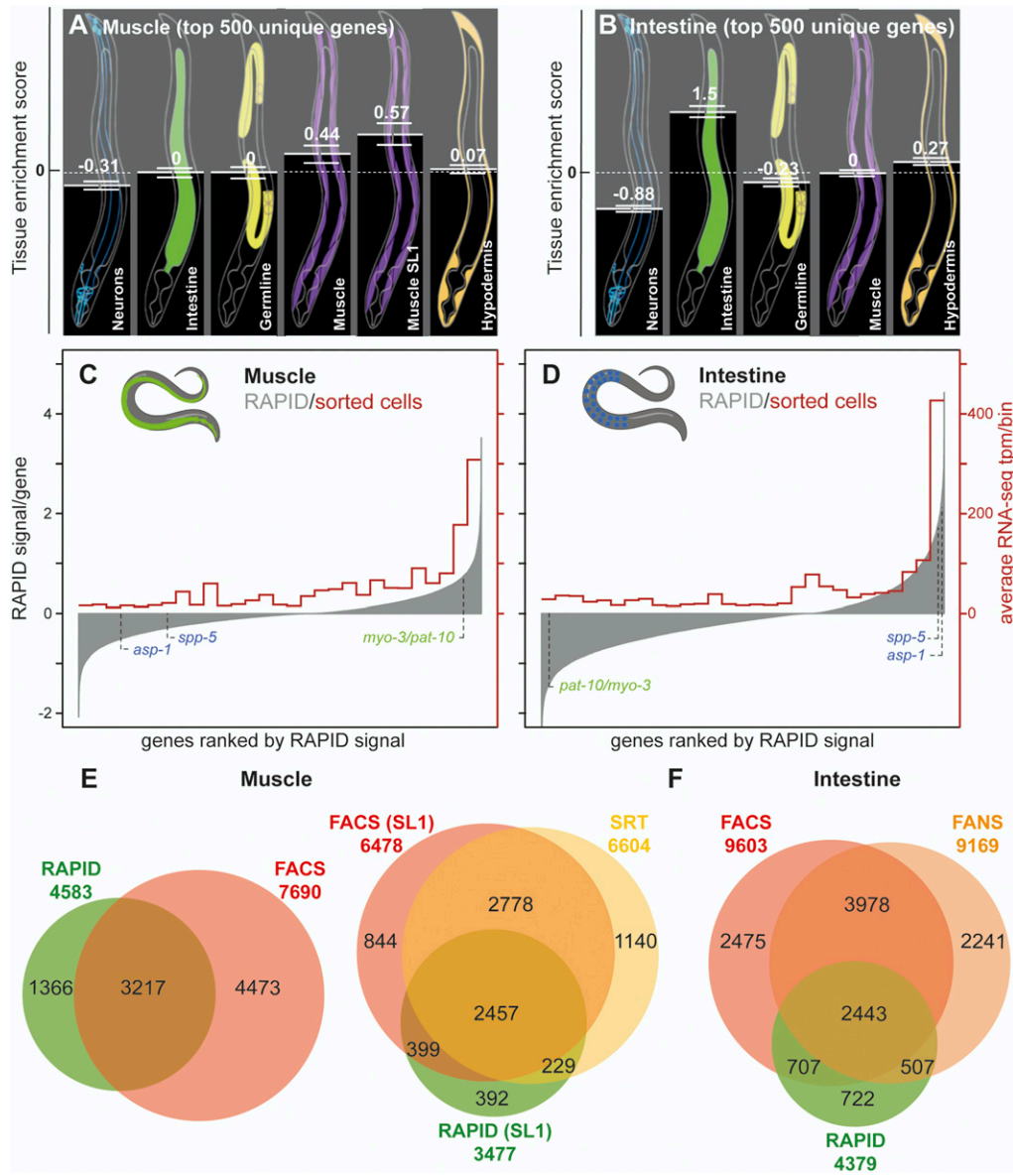


**Figure 3** Validation of RAPID muscular and intestinal transcriptomes. (A and B) Tissue enrichment prediction of tissue-specific RAPID transcriptomes. The top 500 hits of unique tissue-enriched genes for muscle (A) and intestine (B) were analyzed by the online tool Tissue-specific Expression Predictions for *C. elegans* (<http://worm-tissue.princeton.edu/search>). Tissue enrichment scores (mean and SEM) showed that the top genes of each tissue identify their corresponding original tissue. (C and D) Semiquantitative comparison between RAPID and FACS/RNA-seq in intestine and muscle (Kaletsky *et al.* 2018). All genes are represented on the x-axis, ranked from left to right, based on the RAPID signal in the considered tissue (shown on left y-axis). Averages of transcripts per million (tpm) for those genes were calculated, binning genes by pools of 690 (30 bins) on the x-axis (values on right y-axis). The muscular and intestinal marker genes presented in Figure 2C are indicated in green and blue, respectively. (E) Overlap of genes footprinted using RAPID with muscle-expressed genes detected by FACS (left; Kaletsky *et al.* 2018) and SRT (right; Ma *et al.* 2016). For the comparison to SRT data, the subsets of SL1-*trans*-spliced genes detected using RAPID and FACS were used. (F) Overlap of genes footprinted using RAPID with intestine-expressed genes detected by FACS (Kaletsky *et al.* 2018) and FANS (Haenni *et al.* 2012).

contrast, their scores were much lower for nontargeted tissues (including neurons, hypodermis, and germline).

Second, we compared the genome-wide RAPID footprint signal levels with expression levels of genes determined by RNA-seq in FACS-sorted body wall muscle and intestinal cells (Kaletsky *et al.* 2018). As for whole animal samples (Figure 1C), we observed a correlation between RNA-seq levels and RAPID signals for both tissues (Figure 3, C and D). Similar correlations were observed when comparing RAPID signal with scRNA-seq data (Figure S8), with the caveat that the scRNA-seq experiment was performed in the second larval stage, not in young adults (Cao *et al.* 2017).

Third, we compared the RAPID-detected gene sets with those reported for adult muscle and intestine in RNA-seq-based studies [RNA-seq of FACS-sorted cells by Kaletsky *et al.* 2018), SRT (Ma *et al.* 2016), FANS (Haenni *et al.* 2012), or

PAT-seq (Blazie *et al.* 2017)]. A majority of genes with detectable RAPID footprints were also identified with these tissue-specific transcriptomic methods. We found that 90% of the muscle RAPID hits (Figure 3E and Figure S5) and 87% of the intestinal RAPID hits were detected by at least one of the other methods (Figure 3F and Figure S5). Remarkably, the overlap between the genes detected by RAPID and other methods is in the same range as that found between other methods [our own data in Table S5, and similar analyses in Haenni *et al.* (2012); Ma *et al.* 2016]. Although these results are encouraging and suggest that RAPID hits are genuinely expressed in these tissues, we note that the number of genes detected with RAPID is overall lower than that detected with other methods, especially in the intestine, where FACS-sequencing and PAT-seq detect twice as many genes as RAPID (Figure S5C). To evaluate what kind of genes were not

identified by RAPID under our experimental conditions, we performed GO analyses on the common gene sets (identified by two methods) and method-specific gene sets (identified by one but not the other method) (Figures S6 and S7 and Table S6). For this purpose, we used the WormCat analysis tool (Holdorf *et al.* 2020), specifically developed to categorize and visualize *C. elegans* GO data. For the RAPID/FACS and RAPID/PAT-seq common gene sets, we mostly found GO categories related to widely expressed genes (Development, Transmembrane proteins, Signaling, Metabolism...) and categories that one would expect in these tissues (Figures S6 and S7). For example, significantly enriched categories in muscle included Muscle function and Cytoskeleton; and in the intestine, Metabolism of lipids, Trafficking of vesicles, Endocytosis, and Lysosomes (Figure S7). GO categories associated with RAPID-missed genes (only-FACS, only-PAT-seq in Figure S7) and FACS/PAT-seq common genes largely overlapped with those from the RAPID/FACS and RAPID/PAT-seq common genes, and contained additional very general categories (such as Transcription, DNA, Ribosome, Development, or mRNA processing). They also included less expected categories (such as Extracellular material: collagen, Neuronal function: neuropeptide and Major sperm protein in muscle; and Muscle function, Cytoskeleton actin function, and Major sperm protein in intestine). These latter categories may point to possible contaminations by other tissues, a known phenomenon in cell-sorting and cross-linking-based methods (Von Stetina *et al.* 2007; Haenni *et al.* 2012; Spencer *et al.* 2014).

Taken together, the results of our comparative analyses with previous gene expression studies indicate that, even if the number of RAPID-detected genes tends to be lower than for RNA-seq-based methods, RAPID identifies tissue-specific RNA Pol transcriptional activity that largely matches the specific transcriptional output in these tissues.

### **RAPID identifies genes expressed in XXX cells**

XXX cells are neuroendocrine cells derived from hypodermal embryonic progenitors. They express enzymes required for steroid hormone synthesis, such as *DAF-9*, and are implicated in the control of dauer formation during development (Gerisch *et al.* 2001; Ohkura *et al.* 2003). As we still have limited information on the set of genes expressed in XXX cells, as well as on the role of those cells in adults, our XXX cell-transcribed gene data set could represent a valuable resource for future studies. We thus conducted additional experiments to confirm the validity of RAPID profiles to infer gene transcription in those cells and identify new markers.

A GO term analysis highlighted many terms related to secretory and neural functions in the gene set specific for XXX cells, while they were absent from the muscle- and intestine-enriched gene sets (Table S5, sheet 7). These results are expected for neuroendocrine cells, with functional properties very similar to those of neurons.

To further confirm the validity of RAPID profiles to infer gene transcription, we selected 12 genes with high RAPID signal in XXX cells compared to intestine, muscle, and whole

animals, by comparing their profiles in the four tissues (Figure S6). We cloned their putative promoters in front of a mNeon-Green fluorescent reporter (Hostettler *et al.* 2017) and created transgenic lines bearing extrachromosomal arrays by gonad microinjection, together with an XXX-specific red reporter driven by the *sdf-9* promoter (the promoter that we previously used for XXX-specific RAPID). Out of the 12 promoters, 8 drove expression in the XXX cells at various levels (*asic-1*, *dhs-17*, *F14H8.2*, *C06A1.3*, *asp-9*, *B0034.5*, *F52E1.5*, and *nlp-15*; Figure 4), one was impossible to score (*T22E5.6*) because it also drove high expression in the pharynx located very close to the XXX cells, and three did not show detectable expression in XXX cells (in adults; *mab-9*, *twk-39*, and *lgc-36*). The absence of expression in the latter group could indicate that these genes represent false positives in the RAPID analysis, that the transcription was active only at earlier developmental time points, or that the arbitrarily defined promoters failed to reflect the endogenous transcriptional activity. Even if the subset of genes tested with the reporter follow-up analysis is small, we could calculate a gross estimate of the true positive rate of RAPID in XXX cells. Based on the 8:11 ratio (8 positive genes/promoters out of 11 interpretable readouts), a resampling bootstrap simulation indicated that the true positive rate should range between 45 and 88% (95% confidence interval, Figure S10). By extrapolation, this would correspond to a range of ~1100–2100 genes expressed in XXX and identified via RAPID.

Interestingly, in half of the reporters expressed in XXX cells (four out of eight), we observed only limited or no signal in other cell types. In particular, reporters for *dhs-17* and *F14H8.2* were predominantly expressed in XXX cells and sequence homology suggests plausible XXX-specific roles for these two genes. Indeed, *dhs-17* encodes an uncharacterized member of the short-chain dehydrogenase/reductase family, which is potentially involved in steroid metabolism (Zhang *et al.* 2013), and may therefore contribute to this specific neuroendocrine function of XXX cells. As for *F14H8.2*, it is a paralog of *eak-4* selectively expressed in XXX cells and regulating dauer formation (Hu *et al.* 2006).

Taken together, the results of our reporter gene analysis indicate that the RAPID approach applied to only two cells per animal successfully identifies actively transcribed genes in these cells, including genes with relatively low expression and novel cell-specific markers.

### **Discussion**

Determining the transcriptional profile of specific cell types has been a major hurdle for *C. elegans* researchers, as most research is carried out on intact, living animals. Recent technological advances now allow the acquisition of a comprehensive view of the genes expressed in individual cell types. Two main RNA-based approaches have been used in the community to this aim: “RNA tagging/pulling” approaches that allow to sample gene expression directly from whole, live animals, either through affinity purification or pull-down

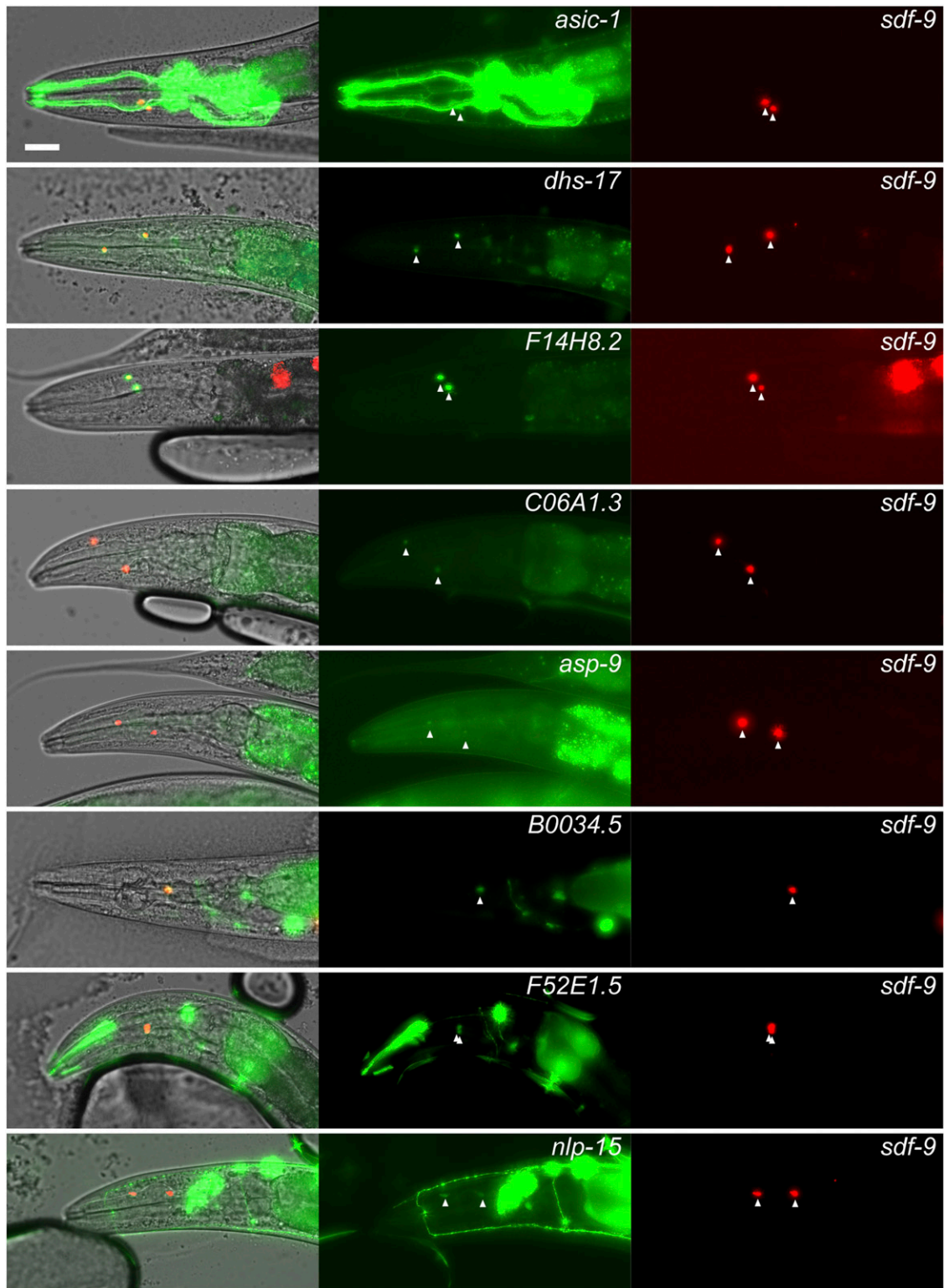


**Figure 4** Promoters of genes identified as expressed in XXX cells using RAPID drive fluorescent reporter expression in XXX cells. Left panel: partial z-projections of adult heads showing expression of *sdf-9p::mScarlet* in XXX cells. Middle panel: partial z-projections of adult heads showing the expression pattern of *mNeonGreen* reporter under transcriptional control of the promoters of indicated genes. Right panel: merge of fluorescent channels within DIC images validating the expression of mentioned genes in XXX cells. Bars, 10  $\mu$ m.

enrichment; and “dissociation-based” methods, requiring tissue dissociation followed by either purification of cells/nuclei by FACS or individual cell isolation.

Here, we adapt a third type of approach originally developed in *Drosophila*, based on RNA Pol footprinting on DNA (Southall *et al.* 2013). RAPID is based on DNA modification by DNA adenine methyltransferase fused with a RNA Pol subunit, detecting active transcribed genes footprinting by DamID (van Steensel *et al.* 2001). RAPID is a simple, fast, and cost-effective technique to identify transcribed genes in individual tissues or cells, requiring only the knowledge of one tissue- or cell-specific promoter. We discuss below the specificities and limits of RAPID for transcriptional profiling, in comparison with previously published methods (summarized in Table S7).

First, as RAPID is based on the extraction of DNA from entire animals, it avoids *in vitro* cell manipulations and cell isolation-induced transcriptome modifications, similarly to RNA-tagging/pulling techniques. Second, since methylation occurs only in cells in which the Dam fusion is expressed after *Cre/lox* recombination, RAPID yields signals with a high specificity toward targeted tissues. Our comparative analyses with other methods for muscle and intestine, as well as the validation of our results with XXX cells, indeed indicate that a majority of RAPID hits are genuinely expressed in these tissues. Third, the very low level of signal background noise in RAPID makes it sensitive enough to function with a low number of worms (4000, at least a 10-fold reduction compared to other methods), even for a tissue representing two cells per animal. This reduces the time necessary for worm population growth. Additionally, as each examined tissue only requires a tissue-specific *Cre* driver (many of which already exist; Kage-Nakadai *et al.* 2014; Ruijtenberg and van den Heuvel 2015), and as the library preparation is relatively simple to execute, RAPID makes it possible to process several conditions/tissues in parallel and is accessible to a neophyte researcher in the field. Fourth, RAPID is versatile, as minimal modifications will be required to target other DNA-interacting proteins, such as transcription factors or chromatin modifiers, to analyze tissue- or cell-specific genome-wide binding (Marshall and Brand 2017; Aughey *et al.* 2018). With the lower cost of nanopore sequencing systems, it is even conceivable that individual laboratories purchase their own equipment, further cutting down on waiting time and indirect costs.

The advantages described above come at a cost, in particular on how quantitative, dynamic, and comprehensive RAPID data are. Our comparison of the overlap between transcriptomic data sets from different methods suggests that a certain portion of genes is uniquely detected by each method (Figure S5), an indication that no single approach truly captures the complete transcriptome or that variable experimental conditions affect the genes identified as expressed. However, when compared to all other RNA-seq based methods (Figure S5), RAPID identified overall less genes as expressed. On the one hand, it is possible that affinity purification or dissociation-based methods could detect a number of genes due to contaminants and experiment-induced gene expression, or stored messengers

inherited from mother cells. On the other hand, RAPID has a number of inherent technical limitations, which may hinder a comprehensive and unbiased genome interrogation.

First, RAPID relies on the GATC density per gene, and a lower density will yield a lower signal, as longer DpnI restriction fragments will be less efficiently amplified by the DamID PCR. In agreement, genes detected using FACS/RNA-seq, but not by RAPID, have on average a lower GATC density (data not shown; Kaletsky *et al.* 2018). Increasing the material amount and/or sequencing coverage is expected to dampen this type of bias. Second, another consequence of the methylation is that the dynamic range of RAPID compared to RNA-seq is expected to be lower: once a gene sequence is fully methylated, further transcription will not lead to increased methylation levels of the DNA, leading to a plateau effect. Conversely, as RAPID uses minute traces of the Dam fusions, lowly expressed genes will rarely be bound by a Pol containing the Dam fusion, and their sequence will be rarely methylated. As our quantitative comparison reveals (Figures 1C and 3B), these issues are partially relieved by the stochasticity of the methylation between different cells in different animals, leading to a correlation between RAPID levels and expression levels determined by RNA-seq. Increasing sequencing coverage should allow both the retrieval of more lowly expressed genes and an improvement in the signal dynamic range. For certain applications, such as identifying tissue-specific genes to serve as molecular markers, a lower dynamic range can actually be an advantage as compared to RNA-seq methods, as the large range of mRNA molecule number in a cell requires very deep sequencing to detect more lowly expressed genes. Third, RAPID signal on DNA will not discriminate between gene isoforms created by alternative splicing, since the RNA Pol will progress over the whole intronic and exonic regions regardless of whether they are retained in the final mRNA product. Fourth, RAPID signal is a stochastic average of the methylation by Pols since the last DNA replication (which erases the methylation signal). The comparison between embryonic blastomeres and young adult tissues (with older postmitotic cells) highlights the increase in reproducibility of RAPID as animals age (Figure S4). Genes detected by RAPID are likely to represent cell-specific genes that are expressed over longer time scales in the cells under study, rather than genes transiently expressed in response to the environment. While this phenomenon enables RAPID to efficiently identify cell-type-specific genes (Tables S4 and S5), it will also limit its ability to report quantitative variations over shorter time scales. Finally, in its present form, RAPID is not well suited to analyze transcriptome dynamics, as the methylation signal can only be erased by DNA replication. RAPID could be further improved by timing the expression of the Dam fusions. We tested auxin-mediated Dam degradation. However, degradation was not complete enough and the remaining low levels of Dam fusions were sufficient to create a RAPID signal (data not shown). Alternatively, degron-tagged *Cre* recombinases might provide a more reliable way to time the expression of the

Dam. In a postmitotic context, however, RAPID should be able to identify transcriptional upregulation events in response to environmental changes, as successfully achieved in *Drosophila* (Widmer *et al.* 2018). In addition, recent publications have highlighted the existence of a large cohort of genes with oscillating expression between molts (Kim *et al.* 2013; Hendriks *et al.* 2014; Hutchison *et al.* 2020; Meeuse *et al.* 2020). RAPID is unlikely to capture this type of phenomenon, which could turn into a desirable feature when one wants to mitigate this variability, *e.g.*, in studies comparing hard-to-synchronize genetic backgrounds.

In conclusion, we believe that RAPID is a useful addition to the existing methods to analyze comprehensive gene expression at the cell-type level, allowing one to identify new and specific markers and further study their biology. RAPID is an easy, scalable, entry-level method to target rare or less known cell types, cell types difficult to purify because of their morphology or the developmental stage targeted, and when synchronization of large populations is tedious, notably when multiple genotypes have to be assessed.

## Acknowledgments

We are grateful to Laurence Bulliard, Cihan Enci, and Lisa Schild for expert technical support; Marc Hammarlund, Piali Sengupta, and Sanders van der Heuvel for the gift of material; and Michalis Barkoulas for sharing preliminary data. Some strains were provided by the CGC (*Caenorhabditis* Genetics Center), which is funded by the National Institutes of Health Office of Research Infrastructure Programs (P40-OD-010440). The study was supported by the Swiss National Science Foundation (grants IZCNZ0-174703/SBFI\_C16.0013, BSSGI0\_155764, and PP00P3\_150681 to D.A.G.; ZCSZ0-174641/SBFI\_C15.0076, PP00P3\_159320, and 31003A\_176226 to P.M.), the ERC CoG (European Research Council Consolidator Grant) PlastiCell grant #648960 to S.J., and a COST Action (European Cooperation in Science and Technology; BM1408).

## Literature Cited

- Allen, M. A., L. W. Hillier, R. H. Waterston, and T. Blumenthal, 2011 A global analysis of *C. elegans* trans-splicing. *Genome Res.* 21: 255–264. <https://doi.org/10.1101/gr.113811.110>
- Aughey, G. N., A. Estacio Gomez, J. Thomson, H. Yin, and T. D. Southall, 2018 CATaDa reveals global remodelling of chromatin accessibility during stem cell differentiation in vivo. *eLife* 7: e32341. <https://doi.org/10.7554/eLife.32341>
- Blazie, S. M., C. Babb, H. Wilky, A. Rawls, J. G. Park *et al.*, 2015 Comparative RNA-seq analysis reveals pervasive tissue-specific alternative polyadenylation in *Caenorhabditis elegans* intestine and muscles. *BMC Biol.* 13: 4. <https://doi.org/10.1186/s12915-015-0116-6>
- Blazie, S. M., H. C. Geissel, H. Wilky, R. Joshi, J. Newbern *et al.*, 2017 Alternative polyadenylation directs tissue-specific miRNA targeting in *Caenorhabditis elegans* somatic tissues. *Genetics* 206: 757–774. <https://doi.org/10.1534/genetics.116.196774>
- Cabianca, D. S., C. Muñoz-Jiménez, V. Kalck, D. Gaidatzis, J. Padenken *et al.*, 2019 Active chromatin marks drive spatial sequestration of heterochromatin in *C. elegans* nuclei. *Nature* 569: 734–739. <https://doi.org/10.1038/s41586-019-1243-y>
- Cao, J., J. S. Packer, V. Ramani, D. A. Cusanovich, C. Huynh *et al.*, 2017 Comprehensive single-cell transcriptional profiling of a multicellular organism. *Science* 357: 661–667. <https://doi.org/10.1126/science.aam8940>
- Chalfie, M., Y. Tu, G. Euskirchen, W. W. Ward, and D. C. Prasher, 1994 Green fluorescent protein as a marker for gene expression. *Science* 263: 802–805. <https://doi.org/10.1126/science.8303295>
- Chikina, M. D., C. Huttenhower, C. T. Murphy, and O. G. Troyanskaya, 2009 Global prediction of tissue-specific gene expression and context-dependent gene networks in *Caenorhabditis elegans*. *PLOS Comput. Biol.* 5: e1000417. <https://doi.org/10.1371/journal.pcbi.1000417>
- Cramer, P., 2004 RNA polymerase II structure: from core to functional complexes. *Curr. Opin. Genet. Dev.* 14: 218–226. <https://doi.org/10.1016/j.gde.2004.01.003>
- Cramer, P., D. A. Bushnell, J. Fu, A. L. Gnat, B. Maier-Davis *et al.*, 2000 Architecture of RNA polymerase II and implications for the transcription mechanism. *Science* 288: 640–649. <https://doi.org/10.1126/science.288.5466.640>
- Frøkjær-Jensen, C., M. W. Davis, C. E. Hopkins, B. J. Newman, J. M. Thummel *et al.*, 2008 Single-copy insertion of transgenes in *Caenorhabditis elegans*. *Nat. Genet.* 40: 1375–1383. <https://doi.org/10.1038/ng.248>
- Garrido-Lecca, A., T. Saldi, and T. Blumenthal, 2016 Localization of RNAPII and 3' end formation factor CstF subunits on *C. elegans* genes and operons. *Transcription* 7: 96–110. <https://doi.org/10.1080/21541264.2016.1168509>
- Gerisch, B., C. Weitzel, C. Kober-Eisermann, V. Rottiers, and A. Antebi, 2001 A hormonal signaling pathway influencing *C. elegans* metabolism, reproductive development, and life span. *Dev. Cell* 1: 841–851. [https://doi.org/10.1016/S1534-5807\(01\)00085-5](https://doi.org/10.1016/S1534-5807(01)00085-5)
- Gómez-Saldivar, G., P. Meister, and P. Askjaer, 2016a DamID analysis of nuclear organization in *Caenorhabditis elegans*. *Methods Mol. Biol.* 1411: 341–358. [https://doi.org/10.1007/978-1-4939-3530-7\\_22](https://doi.org/10.1007/978-1-4939-3530-7_22)
- Gómez-Saldivar, G., P. Meister, and P. Askjaer, 2016b DamID of nuclear envelope proteins in *C. elegans*. *The Nuclear Envelope, Methods and Protocols*, edited by S. Shackleton, P. Collas, and E. C. Schirmer. Springer, Berlin, Germany. pp 341–358 [https://doi.org/10.1007/978-1-4939-3530-7\\_22](https://doi.org/10.1007/978-1-4939-3530-7_22)
- Gracida, X., and J. A. Calarco, 2017 Cell type-specific transcriptome profiling in *C. elegans* using the translating ribosome affinity purification technique. *Methods* 126: 130–137. <https://doi.org/10.1016/j.ymeth.2017.06.023>
- Greer, E. L., M. A. Blanco, L. Gu, E. Sendinc, J. Liu *et al.*, 2015 DNA methylation on N6-adenine in *C. elegans*. *Cell* 161: 868–878. <https://doi.org/10.1016/j.cell.2015.04.005>
- Haenni, S., Z. Ji, M. Hoque, N. Rust, H. Sharpe *et al.*, 2012 Analysis of *C. elegans* intestinal gene expression and polyadenylation by fluorescence-activated nuclei sorting and 3'-end-seq. *Nucleic Acids Res.* 40: 6304–6318. <https://doi.org/10.1093/nar/gks282>
- Hammarlund, M., O. Hobert, D. M. Miller, and N. Sestan, 2018 The CeNGEN project: the complete gene expression map of an entire nervous system. *Neuron* 99: 430–433. <https://doi.org/10.1016/j.neuron.2018.07.042>
- Han, S., E. A. Schroeder, C. G. Silva-García, K. Hebestreit, W. B. Mair *et al.*, 2017 Mono-unsaturated fatty acids link H3K4me3 modifiers to *C. elegans* lifespan. *Nature* 544: 185–190. <https://doi.org/10.1038/nature21686>
- Harr, J. C., C. D. Schmid, C. Muñoz-Jiménez, R. Romero-Bueno, V. Kalck *et al.*, 2020 Loss of an H3K9me anchor rescues laminopathy-linked changes in nuclear organization and muscle function in

- an Emery-Dreifuss muscular dystrophy model. *Genes Dev.* 34: 560–579. <https://doi.org/10.1101/gad.332213.119>
- Hasegawa, K., S. Miwa, T. Tajima, K. Tsutsumiuchi, H. Taniguchi *et al.*, 2007 A rapid and inexpensive method to screen for common foods that reduce the action of acrylamide, a harmful substance in food. *Toxicol. Lett.* 175: 82–88. <https://doi.org/10.1016/j.toxlet.2007.09.013>
- Hendriks, G.-J., D. Gaidatzis, F. Aeschmann, and H. Großhans, 2014 Extensive oscillatory gene expression during *C. elegans* larval development. *Mol. Cell* 53: 380–392. <https://doi.org/10.1016/j.molcel.2013.12.013>
- Holdorf, A. D., D. P. Higgins, A. C. Hart, P. R. Boag, G. J. Pazour *et al.*, 2020 WormCat: an online tool for annotation and visualization of *Caenorhabditis elegans* genome-scale data. *Genetics* 214: 279–294. <https://doi.org/10.1534/genetics.119.302919>
- Hostettler, L., L. Grundy, S. Käser-Pébernard, C. Wicky, W. R. Schafer *et al.*, 2017 The bright fluorescent protein mNeonGreen facilitates protein expression analysis in vivo. *G3 (Bethesda)* 7: 607–615. <https://doi.org/10.1534/g3.116.038133>
- Hrach, H. C., S. O'Brien, H. S. Steber, J. Newbern, A. Rawls *et al.*, 2020 Transcriptome changes during the initiation and progression of Duchenne muscular dystrophy in *Caenorhabditis elegans*. *Hum. Mol. Genet.* 29: 1607–1623. <https://doi.org/10.1093/hmg/ddaa055>
- Hutchison, L. A. D., B. Berger, and I. S. Kohane, 2020 Meta-analysis of *Caenorhabditis elegans* single-cell developmental data reveals multi-frequency oscillation in gene activation. *Bioinformatics* 36: 4047–4057. <https://doi.org/10.1093/bioinformatics/btz864>
- Hu, P. J., J. Xu, and G. Ruvkun, 2006 Two membrane-associated tyrosine phosphatase homologs potentiate *C. elegans* AKT-1/PKB signaling. *PLoS Genet.* 2: e99. <https://doi.org/10.1371/journal.pgen.0020099>
- Ikegami, K., and J. D. Lieb, 2013 Integral nuclear pore proteins bind to Pol III-transcribed genes and are required for Pol III transcript processing in *C. elegans*. *Mol. Cell* 51: 840–849. <https://doi.org/10.1016/j.molcel.2013.08.001>
- Kagawa, H., K. Takuwa, and Y. Sakube, 1997 Mutations and expressions of the tropomyosin gene and the troponin C gene of *Caenorhabditis elegans*. *Cell Struct. Funct.* 22: 213–218. <https://doi.org/10.1247/csf.22.213>
- Kage-Nakadai, E., R. Imae, Y. Suehiro, S. Yoshina, S. Hori *et al.*, 2014 A conditional knockout toolkit for *Caenorhabditis elegans* based on the Cre/loxP recombination. *PLoS One* 9: e114680. <https://doi.org/10.1371/journal.pone.0114680>
- Kagias, K., A. Ahier, N. Fischer, and S. Jarriault, 2012 Members of the NODE (Nanog and Oct4-associated deacetylase) complex and SOX-2 promote the initiation of a natural cellular reprogramming event in vivo. *Proc. Natl. Acad. Sci. USA* 109: 6596–6601. <https://doi.org/10.1073/pnas.1117031109>
- Kaletsky, R., V. Lakhina, R. Arey, A. Williams, J. Landis *et al.*, 2016 The *C. elegans* adult neuronal IIS/FOXO transcriptome reveals adult phenotype regulators. *Nature* 529: 92–96. <https://doi.org/10.1038/nature16483>
- Kaletsky, R., V. Yao, A. Williams, A. M. Runnels, A. Tadych *et al.*, 2018 Transcriptome analysis of adult *Caenorhabditis elegans* cells reveals tissue-specific gene and isoform expression. *PLoS Genet.* 14: e1007559. <https://doi.org/10.1371/journal.pgen.1007559>
- Kalinava, N., J. Z. Ni, K. Peterman, E. Chen, and S. G. Gu, 2017 Decoupling the downstream effects of germline nuclear RNAi reveals that H3K9me3 is dispensable for heritable RNAi and the maintenance of endogenous siRNA-mediated transcriptional silencing in *Caenorhabditis elegans*. *Epigenetics Chromatin* 10: 6. <https://doi.org/10.1186/s13072-017-0114-8>
- Kim, D. H., D. Grün, and A. van Oudenaarden, 2013 Dampening of expression oscillations by synchronous regulation of a microRNA and its target. *Nat. Genet.* 45: 1337–1344. <https://doi.org/10.1038/ng.2763>
- Kunitomo, H., H. Uesugi, Y. Kohara, and Y. Iino, 2005 Identification of ciliated sensory neuron-expressed genes in *Caenorhabditis elegans* using targeted pull-down of poly(A) tails. *Genome Biol.* 6: R17. <https://doi.org/10.1186/gb-2005-6-2-r17>
- Li, H., 2018 Minimap2: pairwise alignment for nucleotide sequences. *Bioinformatics* 34: 3094–3100. <https://doi.org/10.1093/bioinformatics/bty191>
- Lorenzo, R., M. Onizuka, M. Defrance, and P. Laurent, 2020 Combining single-cell RNA-sequencing with a molecular atlas unveils new markers for *Caenorhabditis elegans* neuron classes. *Nucleic Acids Res.* 48: 7119–7134. <https://doi.org/10.1093/nar/gkaa486>
- Marques, F., G. Saro, A.-S. Lia, R. J. Poole, L. Falquet *et al.*, 2019 Identification of avoidance genes through neural pathway-specific forward optogenetics. *PLoS Genet.* 15: e1008509. <https://doi.org/10.1371/journal.pgen.1008509>
- Marshall, O. J., and A. H. Brand, 2015 damidseq pipeline: an automated pipeline for processing DamID sequencing datasets. *Bioinformatics* 31: 3371–3373. <https://doi.org/10.1093/bioinformatics/btv386>
- Marshall, O. J., and A. H. Brand, 2017 Chromatin state changes during neural development revealed by in vivo cell-type specific profiling. *Nat. Commun.* 8: 2271. <https://doi.org/10.1038/s41467-017-02385-4>
- Mattout, A., B. L. Pike, B. D. Towbin, E. M. Bank, A. Gonzalez-Sandoval *et al.*, 2011 An EDMD mutation in *C. elegans* lamin blocks muscle-specific gene relocation and compromises muscle integrity. *Curr. Biol.* 21: 1603–1614. <https://doi.org/10.1016/j.cub.2011.08.030>
- Ma, X., G. Zhan, M. C. Sleumer, S. Chen, W. Liu *et al.*, 2016 Analysis of *C. elegans* muscle transcriptome using trans-splicing-based RNA tagging (SRT). *Nucleic Acids Res.* 44: e156. <https://doi.org/10.1093/nar/gkw734>
- Meeuw, M. W., Y. P. Hauser, L. J. Morales Moya, G.-J. Hendriks, J. Eglinger *et al.*, 2020 Developmental function and state transitions of a gene expression oscillator in *Caenorhabditis elegans*. *Mol. Syst. Biol.* 16: e9498. <https://doi.org/10.15252/msb.20209498>
- Miki, T. S., S. H. Carl, and H. Großhans, 2017 Two distinct transcription termination modes dictated by promoters. *Genes Dev.* 31: 1870–1879. <https://doi.org/10.1101/gad.301093.117>
- Miller, D. M., F. E. Stockdale, and J. Karn, 1986 Immunological identification of the genes encoding the four myosin heavy chain isoforms of *Caenorhabditis elegans*. *Proc. Natl. Acad. Sci. USA* 83: 2305–2309. <https://doi.org/10.1073/pnas.83.8.2305>
- Miyabayashi, T., M. T. Palfreyman, A. E. Sluder, F. Slack, and P. Sengupta, 1999 Expression and function of members of a divergent nuclear receptor family in *Caenorhabditis elegans*. *Dev. Biol.* 215: 314–331. <https://doi.org/10.1006/dbio.1999.9470>
- Mohri, K., and S. Ono, 2003 Actin filament disassembling activity of *Caenorhabditis elegans* actin-interacting protein 1 (UNC-78) is dependent on filament binding by a specific ADF/cofilin isoform. *J. Cell Sci.* 116: 4107–4118. <https://doi.org/10.1242/jcs.00717>
- Muñoz-Jiménez, C., C. Ayuso, A. Dobrzynska, and A. Torres-Mendéz, P. de la Cruz Ruiz *et al.*, 2017 An efficient FLP-based toolkit for spatiotemporal control of gene expression in *Caenorhabditis elegans*. *Genetics* 206: 1763–1778. <https://doi.org/10.1534/genetics.117.201012>
- Ohkura, K., N. Suzuki, T. Ishihara, and I. Katsura, 2003 SDF-9, a protein tyrosine phosphatase-like molecule, regulates the L3/dauer developmental decision through hormonal signaling in *C. elegans*. *Development* 130: 3237–3248. <https://doi.org/10.1242/dev.00540>
- Packer, J. S., Q. Zhu, C. Huynh, P. Sivaramakrishnan, E. Preston *et al.*, 2019 A lineage-resolved molecular atlas of *C. elegans* embryogenesis at single-cell resolution. *Science* 365: eaax1971. <https://doi.org/10.1126/science.aax1971>

- Pauli, F., Y. Liu, Y. A. Kim, P. J. Chen, and S. K. Kim, 2006 Chromosomal clustering and GATA transcriptional regulation of intestine-expressed genes in *C. elegans*. *Development* 133: 287–295. <https://doi.org/10.1242/dev.02185>
- Pindyurin, A. V., L. Pagie, E. N. Kozhevnikova, J. van Arensbergen, and B. van Steensel, 2016 Inducible DamID systems for genomic mapping of chromatin proteins in *Drosophila*. *Nucleic Acids Res.* 44: 5646–5657. <https://doi.org/10.1093/nar/gkw176>
- Raudvere, U., L. Kolberg, I. Kuzmin, T. Arak, P. Adler *et al.*, 2019 Profiler: a web server for functional enrichment analysis and conversions of gene lists (2019 update). *Nucleic Acids Res.* 47: W191–W198. <https://doi.org/10.1093/nar/gkz369>
- Redolfi, J., Y. Zhan, C. Valdes-Quezada, M. Kryzhanovska, I. Guerreiro *et al.*, 2019 DamC reveals principles of chromatin folding in vivo without crosslinking and ligation. *Nat. Struct. Mol. Biol.* 26: 471–480. <https://doi.org/10.1038/s41594-019-0231-0>
- Rhoades, J. L., J. C. Nelson, I. Nwabudike, S. K. Yu, I. G. McLachlan *et al.*, 2019 ASICs mediate food responses in an enteric serotonergic neuron that controls foraging behaviors. *Cell* 176: 85–97.e14. <https://doi.org/10.1016/j.cell.2018.11.023>
- Roeder, T., M. Stanisak, C. Gelhaus, I. Bruchhaus, J. Grötzinger *et al.*, 2010 Caenopores are antimicrobial peptides in the nematode *Caenorhabditis elegans* instrumental in nutrition and immunity. *Dev. Comp. Immunol.* 34: 203–209. <https://doi.org/10.1016/j.dci.2009.09.010>
- Roy, P. J., J. M. Stuart, J. Lund, and S. K. Kim, 2002 Chromosomal clustering of muscle-expressed genes in *Caenorhabditis elegans*. *Nature* 418: 975–979 [corrigenda: *Nature* 450: 128 (2007)]. <https://doi.org/10.1038/nature01012>
- Ruijtenberg, S., and S. van den Heuvel, 2015 G1/S inhibitors and the SWI/SNF complex control cell-cycle exit during muscle differentiation. *Cell* 162: 300–313. <https://doi.org/10.1016/j.cell.2015.06.013>
- Schier, A. C., and D. J. Taatjes, 2020 Structure and mechanism of the RNA polymerase II transcription machinery. *Genes Dev.* 34: 465–488. <https://doi.org/10.1101/gad.335679.119>
- Schuster, E., J. J. McElwee, J. M. Tullet, R. Doonan, F. Matthijssens *et al.*, 2010 DamID in *C. elegans* reveals longevity-associated targets of DAF-16/FoxO. *Mol. Syst. Biol.* 6: 399. <https://doi.org/10.1038/msb.2010.54>
- Sharma, R., D. Jost, J. Kind, G. Gómez-Saldivar, B. van Steensel *et al.*, 2014 Differential spatial and structural organization of the X chromosome underlies dosage compensation in *C. elegans*. *Genes Dev.* 28: 2591–2596. <https://doi.org/10.1101/gad.248864.114>
- Southall, T. D., K. S. Gold, B. Egger, C. M. Davidson, E. E. Caygill *et al.*, 2013 Cell-type-specific profiling of gene expression and chromatin binding without cell isolation: assaying RNA Pol II occupancy in neural stem cells. *Dev. Cell* 26: 101–112. <https://doi.org/10.1016/j.devcel.2013.05.020>
- Spencer, W. C., G. Zeller, J. D. Watson, S. R. Henz, K. L. Watkins *et al.*, 2011 A spatial and temporal map of *C. elegans* gene expression. *Genome Res.* 21: 325–341. <https://doi.org/10.1101/gr.114595.110>
- Spencer, W. C., R. McWhirter, T. Miller, P. Strasbourger, O. Thompson *et al.*, 2014 Isolation of specific neurons from *C. elegans* larvae for gene expression profiling. *PLoS One* 9: e112102. <https://doi.org/10.1371/journal.pone.0112102>
- Steiner, F. A., P. B. Talbert, S. Kasinathan, R. B. Deal, and S. Henikoff, 2012 Cell-type-specific nuclei purification from whole animals for genome-wide expression and chromatin profiling. *Genome Res.* 22: 766–777. <https://doi.org/10.1101/gr.131748.111>
- Takayama, J., S. Faumont, H. Kunitomo, S. R. Lockery, and Y. Iino, 2010 Single-cell transcriptional analysis of taste sensory neuron pair in *Caenorhabditis elegans*. *Nucleic Acids Res.* 38: 131–142. <https://doi.org/10.1093/nar/gkp868>
- Tcherepanova, I., L. Bhattacharyya, C. S. Rubin, and J. H. Freedman, 2000 Aspartic proteases from the nematode *Caenorhabditis elegans*. Structural organization and developmental and cell-specific expression of asp-1. *J. Biol. Chem.* 275: 26359–26369. <https://doi.org/10.1074/jbc.M000956200>
- Towbin, B. D., C. González-Aguilera, R. Sack, D. Gaidatzis, V. Kalck *et al.*, 2012 Step-wise methylation of histone H3K9 positions heterochromatin at the nuclear periphery. *Cell* 150: 934–947. <https://doi.org/10.1016/j.cell.2012.06.051>
- van Steensel, B., J. Delrow, and S. Henikoff, 2001 Chromatin profiling using targeted DNA adenine methyltransferase. *Nat. Genet.* 27: 304–308. <https://doi.org/10.1038/85871>
- Von Stetina, S. E., J. D. Watson, R. M. Fox, K. L. Olszewski, W. C. Spencer *et al.*, 2007 Cell-specific microarray profiling experiments reveal a comprehensive picture of gene expression in the *C. elegans* nervous system. *Genome Biol.* 8: R135. <https://doi.org/10.1186/gb-2007-8-7-r135>
- Wang, J., R. Kaletsky, M. Silva, A. Williams, L. A. Haas *et al.*, 2015 Cell-specific transcriptional profiling of ciliated sensory neurons reveals regulators of behavior and extracellular vesicle biogenesis. *Curr. Biol.* 25: 3232–3238. <https://doi.org/10.1016/j.cub.2015.10.057>
- Widmer, Y. F., A. Bilican, R. Bruggmann, and S. G. Sprecher, 2018 Regulators of long-term memory revealed by mushroom body-specific gene expression profiling in *Drosophila melanogaster*. *Genetics* 209: 1167–1181. <https://doi.org/10.1534/genetics.118.301106>
- Yang, Y.-F., X. Zhang, X. Ma, T. Zhao, Q. Sun *et al.*, 2017 Trans-splicing enhances translational efficiency in *C. elegans*. *Genome Res.* 27: 1525–1535. <https://doi.org/10.1101/gr.202150.115>
- Zhang, Y., X. Zou, Y. Ding, H. Wang, X. Wu *et al.*, 2013 Comparative genomics and functional study of lipid metabolic genes in *Caenorhabditis elegans*. *BMC Genomics* 14: 164. <https://doi.org/10.1186/1471-2164-14-164>

Communicating editor: O. Hobert